[5] J.H. Argyris and G. Mareczek, Thermo-mechanical analysis of structures, Fourth Conf. of the Hungarian Academy of Sciences on Dimensioning and Strength Calculation, Budapest, October 1967, Proceedings pp. 267–285.
[6] R.H. Gallagher and R.H. Mallett, Efficient solution process for finite element analysis of transient heat conduction, Transactions of the ASME, Journal of Heat Transfer (1971) pp. 257–263.
[7] M. Hogge, Analyse numérique des problèmes thermiques en construction aéronautique et spatiale, Thesis, University of Liège, Belgium (1969–1970).
[8] J.H. Argyris, O.E. Brönlund, I. Fried and J.B. Spooner, The changes in the stress distribution round a rectangular hole with rounded corners caused by a varying internal pressure and temperature, Proceedings of the IX. Int. Astronautical Conference, Belgrad, October 1967.
[9] J.H. Argyris and D.W. Scharpf, Finite elements in time and space, Aeron. J. Royal Aeron. Soc. 73 (1969) pp. 1041–1044.
[10] J.H. Argyris, P.C. Dunne and T. Angelopoulos, Non-linear oscillations using finite element technique, Computer Methods in Applied Mechanics and Engineering 2 (1973).
[11] J.D. Lambert, Computational methods in ordinary differential equations (John Wiley, London, 1973).
[12] B.M. Irons, Computer technique: The front solution, prepared for the course on "Application of Variational Techniques in Engineering" (1972) Southampton University, England.
[13] B.M. Irons, A frontal solution program for finite element analysis, International Journal for Numerical Methods in Engineering 2 (1970).
[14] D.D. McCracken and W.S. Dorn, Numerical methods and fortran programming with applications in engineering and science (John Wiley, London, 1964).
[15] J.M. Quitin, Tuyau carré: champ de température en régime transitoire (Calcul par différences finies), not published, Laborelec, 1640 Rhode-St. Genèse, Belgium (1972).
[16] N. Germay and D. van Dommelen, Une nouvelle méthode de calcul de l'échauffement d'un câble enfoui, Revue E, 6 (1969).
[17] N. Germay and D. van Dommelen, Complementary results of a new method for the calculation of buried cable heating, Revue E, no. 12 (1971).
[18] D. van Dommelen, Een nieuwe methode voor de berekening van de opwarming van een ondergrondse kabel en van het omgevend thermisch veld, Thesis, University of Leuven, Belgium (1971).

COMPUTER METHODS IN APPLIED MECHANICS AND ENGINEERING 3 (1974) 269–289

THE NUMERICAL COMPUTATION OF TURBULENT FLOWS

B.E. LAUNDER and D.B. SPALDING
Imperial College of Science and Technology, Department of Mechanical Engineering, Exhibition Road, London, S.W.7, UK

Received 13 August 1973

The paper reviews the problem of making numerical predictions of turbulent flow. It advocates that computational economy, range of applicability and physical realism are best served at present by turbulence models in which the magnitudes of two turbulence quantities, the turbulence kinetic energy k and its dissipation rate ϵ, are calculated from transport equations solved simultaneously with those governing the mean flow behaviour. The width of applicability of the model is demonstrated by reference to numerical computations of nine substantially different kinds of turbulent flow.

Nomenclature

A	Van Driest's constant
C_t	Curtet number defined by (3.1 – 1)
$C_1 C_2 C_\mu C_D$	Coefficients in approximated turbulent transport equations
C_p	Specific heat at constant pressure
D_ϕ	Diffusion coefficient for quantity ϕ
D_{ij}	Rate of diffusive transport of Reynolds stress
E	Constant in near-wall description of velocity profile ($\simeq 9$)
f	Functional defined by (2.2 – 6)
k	Turbulence kinetic energy $\overline{u_i u_i}/2$
l	Length of energy containing eddies
p	Fluctuating component of static pressure
q''	Heat flux
r	Radius
Re	Reynolds number in pipe flow based on bulk velocity and pipe diameter
R_{ij}	Rate of redistribution of Reynolds stress through pressure fluctuations
R_t	Turbulent Reynolds number $k^2/\nu\epsilon$
T	Temperature
u_i	Fluctuating component of velocity in direction x_i
U_i	Mean component of velocity in direction x_i
U^+	Streamwise velocity non-dimensionalized by τ_w/ρ
U_c	Mean streamwise velocity on axis
ΔU	Change in mean velocity across shear flow
W	'Vorticity' fluctuations squared
x_i	Cartesian space coordinate

Y	Radial width of mixing region
y	Coordinate normal to wall

Greek Symbols

ϵ	Rate of dissipation of turbulence energy
κ	von Karman's constant appearing in (2.1 – 11)
μ	Molecular viscosity
μ_t	Turbulent viscosity
ν	Kinematic viscosity
ϕ	A generalized dependent variable
ρ	Density
σ_t	Effective turbulent Prandtl number
σ_ϕ	Effective turbulent Prandtl number for transport of ϕ
σ_h	Molecular Prandtl number
τ	Shear stress

Subscripts

$i\,j\,k$	Subscripts denoting Cartesian coordinate directions
i	Inner surface
o	Outer surface
p	Value at a node adjacent to the wall
w	Wall value

Superscript

$+$	Denotes quantity non-dimensionalized by means of ν, τ_w, and ρ

1. Introduction

1.1. The Problem

Turbulent flows, which are of great practical importance, are three-dimensional and time-dependent. Computer methods of solving the differential equations of fluid dynamics are well advanced even for three-dimensional time-dependent flows. Then why is it that there are no computer models of turbulent flow which do full justice to the fluid dynamics and which can be applied to practical problems?

The answer is that the necessary computer storage exceeds by many orders of magnitude what is currently available, to say nothing of the computer time, for important constituents of the turbulence phenomenon take place in eddies of the order of a millimeter in size, while the whole flow domain may extend over meters or kilometers. A grid fine enough to allow accurate description of a turbulent flow would therefore require an immense and totally impractical number of nodes.

Yet the practical need for computation of turbulent flows is pressing; to meet it, "turbulence models" have been invented. These consist of sets of differential equations, and associated algebraic equations and constants, the solutions of which, in conjunction with those of the Navier–Stokes equations, closely simulate the behaviour of real turbulent fluids.

A good turbulence model has extensive universality, and is not too complex to develop or use. Universality implies that a single set of empirical constants or functions, inserted into the equations, provides close simulation of a large variety of types of flow. Complexity is measured by the number of differential equations which the model contains, and the number of the empirical constants and functions which are required to complete them; increase in the first complicates the task of using the model, increase in the second that of developing it.

Satisfactory calculation procedures and computers are now available for solving differential equations, on the scale of the mean motion, for quite large numbers (e.g. 20) of simultaneous equations. The main obstacles to model development are therefore the difficulty of selecting which set of differential equations is most capable of providing universality, and the difficulty of then providing, from experimental knowledge, the required constants and functions.

1.2. Purpose of the present paper

In the present paper, the authors describe recent work on the development of a particular turbulence model, that in which two differential equations are solved, the dependent variables of which are the turbulence energy k and the dissipation rate of turbulence energy ϵ. Emphasis is given to aspects of the model having importance for flows adjacent to solid walls.

This is of course not the only available turbulence model. Others have been reviewed in recent works by the authors [1, 2] and others (Harlow [3] and Mellor and Herring [4]).

Among such models are:-

Prandtl's [5] mixing-length model; the one-differential-equation models of Prandtl [6], Bradshaw, Ferriss and Atwell [7] and Nee and Kovasznay [8]; the two-differential-equation models of Kolmogorov [9], Harlow and Nakayama [10], Spalding [11], and Jones and Launder [12]; and the more complex models of Chou [13], Rotta [14], Davidov [15], Kolovandin and Vatutin [16], Hanjalić [17] and Hanjalić and Launder [18].

Recently, a conference was devoted to comparison of the predictions of various models, with each other and with experiment, for certain turbulent-flow phenomena remote from walls. The $k \sim \epsilon$ model was there shown, by Launder, Morse, Rodi and Spalding [19], to be surpassed only by admittedly more complex "Reynolds-stress" models, which are still not completely developed. It therefore seems appropriate to present a more detailed description of the $k \sim \epsilon$ model than has been available hitherto, and to review recent predictions which have been made with its aid.

The paper will concentrate attention on the differential equations and auxiliary relations which define the model, and on their solutions. The solution procedures will not be described here, because they are standard ones, published by Patankar and Spalding [20] and Gosman, Pun, Runchal, Spalding and Wolfshtein [21].

2. The $k \sim \epsilon$ model

2.1. The reason for its choice

The authors and their colleagues have had experience with three different kinds of two-equation turbulence model: $k \sim kl$, $k \sim W$, and $k \sim \epsilon$. Here k stands for the turbulence energy:

$$k \equiv \tfrac{1}{2}\overline{u_i u_i}\ ; \tag{2.1–1}$$

l is a length representing the macroscale of turbulence, which we may define in terms of k, ϵ, and a constant C_D through:

$$l = C_D k^{3/2}/\epsilon\ ; \tag{2.1–2}$$

W is a quantity having the dimensions of (time)$^{-2}$, which has been interpreted (Spalding [22]; Saffmann [23]) as representing the time-average square of the vorticity fluctuations and which can also be defined in terms of k, ϵ, and C_D through:

$$W = \epsilon^2/(C_D k)^2\ ; \tag{2.1–3}$$

and ϵ is defined by:

$$\epsilon = \nu \overline{\frac{\partial u_i}{\partial x_k}\frac{\partial u_i}{\partial x_k}}\ ; \tag{2.1–4}$$

where ν is the kinematic viscosity of the fluid.

Papers describing the $k \sim kl$ model and its application to a large number of turbulent flows, both with and without the presence of solid walls, are those of Rodi and Spalding [24], and Ng and Spalding [25, 26]. The $k \sim W$ model has been described in papers by Spalding [11, 22, 27] and Gibson and Spalding [28]; a similar model was proposed independently by Saffmann [23]. A form of $k \sim \epsilon$ model was first proposed by Harlow and Nakayama [10], and has appeared also in the papers of Jones and Launder [12, 29] and Launder et al. [19].

The definitions (2.1–2) and (2.1–3) above imply:

$$\frac{\mathrm{d}kl}{kl} = \frac{5}{2}\frac{\mathrm{d}k}{k} - \frac{\mathrm{d}\epsilon}{\epsilon}\ ; \tag{2.1–5}$$

$$\frac{\mathrm{d}W}{W} = -2\frac{\mathrm{d}k}{k} + 2\frac{\mathrm{d}\epsilon}{\epsilon}\ ; \tag{2.1–6}$$

With the aid of these equations, it is easily possible to turn a pair of equations for k and kl say, into a pair of equations for k and W, or another pair for k and ϵ. Therefore, one might regard the various two-equation models as differing merely in mathematical form, and not in content. Despite this, there are cogent reasons for preferring the $k \sim \epsilon$ model, as follows.

First, in the absence of superior knowledge, all third-order correlations which appear in the transport equations must be represented by way of gradients of the dependent variable of the relevant equation. Thus, for example,

$$-\frac{\partial}{\partial x_i}\left[u_i \frac{(u_j u_j}{2} + \frac{p)}{\rho}\right]$$

is represented by:

$$\frac{\partial}{\partial x_i}\left[D_k \frac{\partial k}{\partial x_i}\right]$$

where D_k is an effective diffusion coefficient for the turbulence energy k. Now it is not possible to transform an expression such as

$$\frac{\partial}{\partial x_i}\left[D_k \frac{\partial k}{\partial x_i}\right]$$

into a similar expression involving ϵ as dependent variable, without introducing gradients of k into the equation. Thus, if physical realism demands that the only second-order differential coefficient in the kl equation should be that involving kl itself, there must be *two* such coefficients in the equation for ϵ; and vice versa.

Secondly, there is no knowledge, at present, of whether the transport of kl, W or ϵ is the more correctly represented by a single second-order term; and one reason for this lack of knowledge is that, in the free turbulent flows (jets, wakes, etc.) that have been most widely studied, the length scale is found to be nearly uniform across the flow. As further manipulation of (2.1–5) and (2.1–6) easily reveals, if $\mathrm{d}l$ is nearly zero, there follows:

$$\frac{\mathrm{d}kl}{kl} \approx \frac{\mathrm{d}k}{k} \tag{2.1–7}$$

$$\frac{\mathrm{d}W}{W} \approx \frac{\mathrm{d}k}{k} \tag{2.1–8}$$

$$\frac{\mathrm{d}\epsilon}{\epsilon} \approx \frac{3}{2}\frac{\mathrm{d}k}{k} \tag{2.1–9}$$

so that error-free transformation of one model into another is nearly possible.

Thirdly however, it is known that, in the region close to a wall where the shear stress τ is uniform, the length scale increases linearly with distance from the wall. Now, in such a region the differential equation governing the variable k^m/l^n (adopted for the moment as a generalization of k, $W\,(=k/l^2)$ and $\epsilon\,(=k^{3/2}/l)$) typically reduces to:

$$0 = \frac{\partial}{\partial x_2}\left[\frac{\mu_t}{\sigma_t}\frac{\partial(k^m/l^n)}{\partial x_2}\right] + C_1 \mu_t \frac{k^{m-1}}{l^n}\left(\frac{\partial U_1}{\partial x_2}\right)^2 - C_2 \frac{\rho k^{m+1/2}}{l^{n+1}} \tag{2.1–10}$$

the convection terms having vanished and σ_t introduced now to represent the Prandtl number for the turbulent transport of k^m/l^n. Further, because the energy is uniform and the length scale l is proportional to the distance from the wall x_2, this differential equation reduces to an algebraic relation between the constants, namely:

$$\frac{n^2}{\sigma_t} + \frac{C_1 C_\mu^{1/2}}{\kappa^2} - \frac{C_2 C_\mu^{1/2}}{\kappa^2} = 0 \qquad (2.1\text{–}11)$$

where κ is von Karman's constant, appearing in the "logarithmic law of the wall":

$$\frac{U_1}{(\tau/\rho)^{1/2}} = \frac{1}{\kappa} ln \left[\frac{E x_2 (\tau/\rho)^{1/2}}{\nu} \right]. \qquad (2.1\text{–}12)$$

In developing (2.1–11), equation (2.1–12) has been substituted into (2.1–10), as has also the relation defining the effective turbulent viscosity μ_t, namely:

$$\mu_t = C_\mu \rho k^{1/2} l \qquad (2.1\text{–}13)$$

where ρ is the fluid density.

It is now possible to explain the main reason for preferring the $k \sim \epsilon$ model (for which $n = +1$) to the $k \sim W$ model (for which $n = +2$) and to the $k \sim kl$ model (for which $n = -1$): when the proper values of C_μ, C_1, C_2 * and κ are inserted into the equation (2.1–11), the resulting value of σ_t is -0.8 for the $k \sim kl$ model, 2.9 for the $k \sim W$ model and 1.3 for the $k \sim \epsilon$ model; and *only the latter value is of a magnitude which will fit the experimental data for the spread of the various entities at locations far from walls.* Because of this, the developers of the $k \sim kl$ and $k \sim W$ models have to propose that one or more of the "constants", perhaps σ_t itself, should vary with the non-dimensional ratio x_2/l; only for the $k \sim \epsilon$ model is this adjustment, which is hard to base securely on experimental data, rendered unnecessary.

Of course, it may be that some of the "constants" *should* depend upon x_2/l; and perhaps also the true behaviour of turbulence requires that gradients of more than one turbulence property drive diffusional effects. However, until theoretical or experimental evidence of this is forthcoming, it seems better to stand by the simplest formulations.

2.2. Recommended Constants and Functions

At high Reynolds numbers, the transport equation for ϵ may be expressed:

$$\frac{D\epsilon}{Dt} = \frac{1}{\rho} \frac{\partial}{\partial x_k} \left[\frac{\mu_t}{\sigma_\epsilon} \frac{\partial \epsilon}{\partial x_k} \right] + \frac{C_1 \mu_t}{\rho} \frac{\epsilon}{k} \left(\frac{\partial U_i}{\partial x_k} + \frac{\partial U_k}{\partial x_i} \right) \frac{\partial U_i}{\partial x_k} - C_2 \frac{\epsilon^2}{k} \qquad (2.2\text{–}1)$$

a form which was first developed and used in the Imperial College group by Hanjalić [17]. Equation (2.2–1) together with a similar one for the turbulence energy, k:

$$\frac{Dk}{Dt} = \frac{1}{\rho} \frac{\partial}{\partial x_k} \left[\frac{\mu_t}{\sigma_k} \frac{\partial k}{\partial x_k} \right] + \frac{\mu_t}{\rho} \left(\frac{\partial U_i}{\partial x_k} + \frac{\partial U_k}{\partial x_i} \right) \frac{\partial U_i}{\partial x_k} - \epsilon \qquad (2.2\text{–}2)$$

enables the turbulent viscosity μ_t to be found from equation (2.1–13) or its equivalent in terms

* The values of C_1 and C_2 depend on the choices for m and n.

of ϵ (rather than l); thus:

$$\mu_t = C_\mu \rho k^2 / \epsilon \,. \qquad (2.2\text{–}3)$$

According to the recommendations of Launder et al. [19], made after extensive examination of free turbulent flows, the constants appearing in equations (2.2–1)–(2.2–3) take the values given in table 2.1:

Table 2.1
The values of the constants in the $k \sim \epsilon$ model

C_μ	C_1	C_2	σ_k	σ_ϵ
0.09	1.44	1.92	1.0	1.3

The above constants have been found appropriate to plane jets and mixing layers. Slightly different values from those quoted have hitherto been adopted in the calculation of flows near walls; but there is reason to suppose that, for these flows also, the values in table 2.1 would lead to as satisfactory preditions as obtained with those originally employed.

For *axisymmetric jets* it is, regrettably, necessary to modify two of the constants; continued efforts have failed to devise any single set of constants that will predict their behaviour as well as that of the plane free shear flows and the plane or axisymmetric wall flows. The following recommendation has therefore been made by Launder et al. [19] based on the work of Rodi [30].

$$C_\mu = 0.09 - 0.04 f \qquad (2.2\text{–}4)$$

$$C_2 = 1.92 - 0.0667 f \qquad (2.2\text{–}5)$$

where

$$f = \left| \frac{Y}{2\Delta U} \left(\frac{\partial U_{cl}}{\partial x_1} - \left| \frac{\partial U_{cl}}{\partial x_1} \right| \right) \right|^{0.2} . \qquad (2.2\text{–}6)$$

Here reference is made to U_{cl}, the velocity at, and in the direction of, the symmetry axis of the flow; Y is the radial width of the mixing region, and ΔU is the axial-direction velocity difference across the width of this region.

This recommendation is especially tailored to fit the experimental data for axisymmetrical jets * and little universality can trully be claimed for it. (For example, if a thin wire lay along the axis of the jet, U_{cl} would be made zero thereby; yet it seems unlikely that the spread of the jet would be significantly altered). However, it is the best available at the present time. Rodi [30] has found that a further modification of the constants is required in turbulent flows where velocity gradients are so weak that the rate of turbulence-energy generation is appreciably less than the energy-dissipation rate. Examples of such flows are wakes at very large distances behind the wake generators and the decaying flow behind a self-propelled body. In these cases C_μ assumes higher values than

* For wakes the form of (2.2–4) renders f zero.

the standard one: Rodi [30] has correlated the required magnitude of C_μ as a function of the average level of $\mu_t(\partial U_i/\partial x_k)^2/\rho\epsilon$ across the wake.

Although the weak shear flows mentioned above are not without their practical importance, it needs to be emphasized that the great majority of flows of interest to the mechanical engineer are ones adjacent to, and often enclosed by, rigid surfaces. The presence of a wall enforces steep velocity gradients; consequently the level of turbulence-energy production is always large; the values of the constants given in table 2.1 are therefore nearly always applicable.

2.3. The influence of a nearby wall

The form of the model which has been presented above is valid only for fully turbulent flows. Close to solid walls, and some other interfaces, there are inevitably regions where the local Reynolds number of turbulence ($\equiv k^{1/2}l/\nu$, where $l \equiv k^{3/2}/\epsilon$) is so small that viscous effects predominate over turbulent ones. There are two methods of accounting for these regions in numerical methods for computing turbulent flow: the wall-function-method; and the low-Reynolds-number-modelling method. We shall now discuss these in turn.

2.3–1. The wall-function method

This method is the one which has been most widely used, and which is indeed still to be preferred for many practical purposes. Its merits are two: it economizes computer time and storage; and its allows the introduction of additional empirical information in special cases, as when the wall is rough.

Wall functions have been proposed and used by many authors including Spalding [31], Wolfshtein [32] and Patankar and Spalding [20]. The ones proposed here represent the best practice of the Imperial College group; but it must be admitted that further systematic research must be conducted before they can be regarded as having been tested adequately. They will first be described, and then their rationale will be explained.

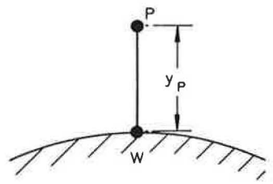

Fig. 2.1. The near-wall nodes.

Consider the adjacent grid points W and P of a finite-difference grid on which the flow is to be computed (fig. 2.1). The first feature to make sure of, when using the wall-function method, is that the point P is sufficiently remote from W, which lies on the wall, for $(k^{1/2}l/\nu)_P$ to be much greater than unity; so much greater in fact that the viscous effects are entirely overwhelmed there by the turbulent ones.

The fluxes of momentum and heat to the wall are then supposed to obey the relations:

$$\frac{U_p}{(\tau/\rho)_w} C_\mu^{1/4} k_p^{1/2} = \frac{1}{\kappa} ln \left[E y_p \frac{(C_\mu^{1/2} k_p)^{1/2}}{\nu} \right] \tag{2.3–1}$$

$$\frac{(T_p - T_w) C_p \rho C_\mu^{1/4} k_p^{1/2}}{\dot{q}_w''} = \frac{\sigma_h}{\kappa} ln \left[\frac{E y_p (C_\mu^{1/2} k_p)^{1/2}}{\nu} \right] + \sigma_h \frac{\pi/4}{\sin \pi/4} \left(\frac{A}{k}\right)^{1/2} \left(\frac{\sigma_{h,l}}{\sigma_h} - 1\right) \left(\frac{\sigma_h}{\sigma_{h,l}}\right)^{1/4} . \tag{2.3–2}$$

Here U_p, τ_w, T_p, T_w, $\dot{q}_w''$, and y_p are respectively the time-average velocity of the fluid at point P along the wall, the shear stress on the wall in the direction of the velocity U_p, the time-average temperatures of the fluid at points P and W respectively, the heat flux to the wall, and the distance of the point P from the wall.

Other symbols appearing in the equation have the following meanings:

E a function of the wall roughness, approximately equal to 9.0 for a smooth wall;

C_p the constant-pressure specific heat of the fluid;

σ_h the effective Prandtl number of the fully turbulent fluid (usually taken as being of the order of 1);

$\sigma_{h,l}$ the Prandtl number of the wholly laminar fluid;

A Van Driest's constant, equal to 26.0 for a smooth wall.

The quantity k_p, the value of k for the grid point, is supposed to be known. It should be calculated from the regular balance equation of the finite-difference grid, diffusion of energy to the wall being set equal to zero (in the absence of better information). When calculating k_p, it is of course necessary to assign a value for the average energy-dissipation rate over the control volume; this is to be deduced from the assumption that:

$$\int_0^{Y_P} \epsilon \, dy = C_\mu \frac{k_p^{3/2}}{\kappa} ln \left[\frac{E y_p (\sqrt{C_\mu^{1/2}} k_p)^{1/2}}{\nu} \right] \tag{2.3–3}$$

The rationale of these recommendations comprises the following main points:

(a) The wall functions reproduce identically the full implications of the "logarithmic velocity profile" when uniform shear stress prevails in the layer WP, and generation and dissipation of energy are in balance there; for then, as is easily shown, $\tau/\rho = C_\mu^{1/2} k$ = constant.

(b) The second term on the right of equation (2.3–2) has its origin in an analysis of experimental data conducted by Jayatillaka [33]. Further information is to be found in [1].

(c) The appearance of the logarithmic function in (2.3–3) results from the necessity to presume ϵ to be proportional to $k^{3/2}/y$, coupled with a further modelling of the wall function on the constant-shear-stress situation.

The extra empirical information which can be inserted by way of wall functions is expressed by way of the constants or functions E and A. Not only can roughness be accounted for, but also such phenomena as pressure gradient and mass transfer through the wall. When the "wall" is slightly flexible, as is true of the interface between two immiscible liquids, further influences are present which can, perhaps, be expressed by way of the formulae. However, there is much research to do in this branch of turbulence-model theory.

2.3–2. The low-Reynolds-number modelling method

Several authors have sought to devise turbulence-model equations which are valid throughout the laminar, semi-laminar, and fully turbulent regions. They include Glushko [34] and Wolfshtein [32], both of whom worked with one-equation turbulence models. We here summarize the recommendations of Jones and Launder [12, 29], who extended the $k \sim \epsilon$ model to low-Reynolds-number flows.

In this version of the model, k and ϵ are determined from the following pair of equations:

$$\frac{D\epsilon}{Dt} = \frac{1}{\rho}\frac{\partial}{\partial x_j}\left[\left(\frac{\mu_t}{\sigma_\epsilon}+\mu\right)\frac{\partial \epsilon}{\partial x_j}\right] + C_1\frac{\epsilon}{k}\frac{\mu_t}{\rho}\frac{\partial U_i}{\partial x_j}\left(\frac{\partial U_i}{\partial x_j}+\frac{\partial U_j}{\partial x_i}\right) - \frac{C_2\epsilon^2}{k} - 2.0\,\frac{\nu\mu_t}{\rho}\left(\frac{\partial^2 U_i}{\partial x_j \partial x_l}\right)^2 \qquad (2.3\text{–}4)$$

$$\frac{Dk}{Dt} = \frac{1}{\rho}\frac{\partial}{\partial x_j}\left[\left(\frac{\mu_t}{\sigma_k}+\mu\right)\frac{\partial k}{\partial x_j}\right] + \frac{\mu_t}{\rho}\frac{\partial U_i}{\partial x_j}\left(\frac{\partial U_i}{\partial x_j}+\frac{\partial U_j}{\partial x_i}\right) - 2\nu\left(\frac{\partial k^{1/2}}{\partial x_j}\right)^2 - \epsilon\,. \qquad (2.3\text{–}5)$$

The turbulent viscosity is then obtained from equation (2.2–3). In the above equation C_1, σ_k and σ_ϵ retain the values assigned to them for high Reynolds numbers, while C_μ and C_2 are held to vary with turbulence Reynolds number according to the formulae:

$$C_\mu = C_{\mu\infty}\exp\left[-2.5/(1+R_t/50)\right], \qquad (2.3\text{–}6)$$

$$C_2 = C_{2\infty}\left[1.0 - 0.3\exp -R_t^2\right], \qquad (2.3\text{–}7)$$

where R_t denotes the turbulence Reynolds number and $C_{\mu\infty}$ and $C_{2\infty}$ are the values assumed by C_μ and C_2 in the fully turbulent region, i.e. the values given in table 2.1 *.

It is seen from (2.3–4) and (2.3–5) that viscosity now exerts influence on the levels of k and ϵ in two further ways: firstly laminar diffusive transport becomes of increasing importance as the wall is approached and, secondly, extra destruction terms have been included which are of some significance in the viscous and transitional regions. One of these terms,

$$2.0\,\frac{\nu\mu_t}{\rho}\left(\frac{d^2U_l}{dx_j dx_l}\right)^2$$

has been included in the ϵ equation to produce satisfactory variation of k with distance from the wall.

The extra term in the k equation, $-2\nu(dk^{1/2}/dx_j)^2$, has been introduced for computational rather than physical reasons. Measurements indicate that the level of the turbulence energy dissipation rate is constant in the immediate neighbourhood of a wall (i.e. for $x_2(\tau/\rho)^{1/2}/\nu < 5$). We could, in principle, thus apply a zero-gradient boundary condition to the ϵ equation at the surface. In practice, however, Jones and Launder [12] did not find this a tractable route; with this

* The values of C_1 and C_2 adopted by Jones and Launder [12] (1.55 and 2.0 respectively) differ slightly from those given in table 2.1. As mentioned above, however, in wall flows generation and decay rates of turbulence energy are nearly in balance and then it is mainly the *difference* between these constants that is influential; and the difference is very nearly the same as for the standard constants. So predictions obtained with the constants of table 2.1 would differ only slightly from those obtained for the same flow using the values given by Jones and Launder.

boundary condition they were unable to devise a compatible set of Reynolds-number functions. Instead the practice adopted was to assign the quantity ϵ to zero at the wall and to introduce to the k equation the extra term mentioned above which is exactly equal to the energy dissipation rate in the neighbourhood of the wall.

2.4. Extension to flows with non-isotropic effective transport coefficients

The form of the $k \sim \epsilon$ model presented so far has by implication adopted the notion of a *scalar* turbulent viscosity.

$$-\overline{\rho u_i u_j} = \mu_t\left[\frac{\partial U_i}{\partial x_j}+\frac{\partial U_j}{\partial x_i}\right] - \tfrac{2}{3}\rho\delta_{ij}k\,. \qquad (2.4\text{–}1)$$

This supposition has proved prefectly adequate in two-dimensional flows without swirl, where only one stress component exerts much influence on the flow development. In flows with swirl, however, and indeed in three-dimensional flows generally, evidence is accumulating (e.g. Roberts [35]) to indicate that the measured flow distribution can be predicted in detail only by choosing a different level of viscosity for each active stress component. None of the workers who has sought to extend (2.4–1) to include non-isotropic effects has succeeded in devising rules for calculating the relevant viscosity components that cover even the limited range of flows in their enquiries.

In this section we mention an extension of the $k \sim \epsilon$ model which, though of recent origin and not yet thoroughly tested, evidently provides a more generally valid formula connecting the stress and strain fields than the effective viscosity hypothesis above. The approach is described in detail by Launder [36] and Rodi [30]; applications of the procedure have been reported by Launder and Ying [37, 38] to the flows in square-sectioned ducts, by Rodi [30] to obtain the normal-stress profiles in some free-shear flows, and by KooSinLin and Lockwood [39] to the calculation of flows near rotating cones and discs. The main steps are outlined below.

The starting point in deriving the relevant stress-strain formulae is the exact equation for the transport of Reynolds stress which may be written:

$$\frac{\overline{Du_i u_j}}{Dt} = -\left[\overline{u_i u_k}\frac{\partial U_j}{\partial x_k} + \overline{u_j u_k}\frac{\partial U_i}{\partial x_k}\right] + D_{ij} + \epsilon_{ij} + R_{ij} \qquad (2.4\text{–}2)$$

where the first group of terms on the right of (2.4–2) represents the generation of the stress component $\overline{u_i u_j}$ by the working of this and other stress components against mean velocity gradients and where D_{ij}, ϵ_{ij}, and R_{ij} stand for turbulence correlations whose values are not directly knowable but whose effects are, respectively, diffusive, dissipative and redistributive. The current practice in approximating these terms is to assume that:

(i) diffusional transport is proportional to the spatial gradient of the stress component in question;

(ii) dissipation takes place isotropically in each of the three normal-stress components and is zero in the shear-stress equations;

(iii) the redistributive action of pressure fluctuations can be represented by two groups of terms, one involving products of Reynolds stress and (ϵ/k); the other containing products of the stresses and mean velocity gradients.

Further details on precise forms of the above approximations are given by Launder, Reece and Rodi [40]. What is especially important in the present context is that the approximation of neither ϵ_{ij} nor R_{ij} contain *gradients* of stress components. The essence of "algebraic" stress modelling then resides in the recognition that if the terms $\overline{Du_iu_j}/Dt$ and D_{ij} are eliminated from (2.4–2) the equation is thereby reduced from a differential to an algebraic set of equations among the Reynolds stresses, the turbulence energy, the energy dissipation rate and mean velocity gradients. Thus expressed symbolically:

$$\overline{u_iu_j} = f\left(\overline{u_pu_q}, k, \epsilon, \frac{\partial U_l}{\partial x_m}\right). \qquad (2.4\text{–}3)$$

Research has not yet revealed the optimum form that the function in (2.4–3) should take. Its appearance will depend on the approximated form of R_{ij} and ϵ_{ij} and on how the convective and diffusive transport terms are eliminated from (2.4–2). Launder [36] neglected the latter terms entirely while Rodi [30] assumed that convective transport of $\overline{u_iu_j}$ was proportional to Dk/Dt times $\overline{u_iu_j}/k$, with an equivalent assumption for the diffusion term. In complicated velocity fields these terms are rarely the most influential ones; so in practice only small differences result from adopting one of the above proposals rather than the other.

What is certainly the case is that the algebraic form of (2.4–3) is always more complex than the isotropic viscosity formula (2.4–1); but, for boundary-layer flows, the additional complexity increases only slightly the cost of computation. The turbulence energy and dissipation rate appearing in (2.4–3) may be found from the pair of differential equations presented in section 2.2; this is the simpler practice. Alternatively one may use the values of $\overline{u_iu_j}$ obtained from (2.4–3) to replace $\mu_t(\partial U_i/\partial x_j + \partial U_j/\partial x_i)$ which appears in the generation terms of these equations; this would be a more consistent practice and probably a more accurate one too.

3. Some Applications of the $k \sim \epsilon$ model

3.1. The plane jet in a moving stream

An example of the predictions generated by the $k \sim \epsilon$ model in a free shear flow is presented in fig. 3.1 from the work of Launder et al. [19]. It relates to the decay of a plane jet in a moving stream, the experimental data being those of Bradbury [41]. Predictions are shown for the $k \sim \epsilon$ model and for two simpler treatments; one based on Prandtl's [5] mixing-length hypothesis and another similar to his later proposal [6] in which a differential equation was provided for k (but not for l).

Predictions obtained with the $k \sim \epsilon$ model are in satisfactory agreement with experiment throughout the region of measurement. The simpler models, however, fail to predict correctly the development of the shear flow much beyond the end of the potential core. Of course, the constants in these models could have been adjusted to give better downstream agreement; but only by sacrificing the good agreement in the mixing-layer region near the jet exit. The two-equation level is the simplest at which universality is secured for both jet and mixing layer.

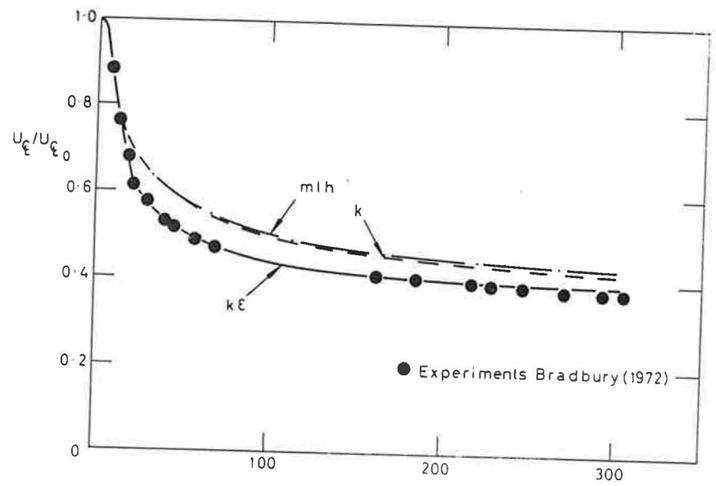

Fig. 3.1. Decay of centre line velocity in jet in moving stream.

3.2. Wall jets on cones

In the above example the solution of the mean momentum and turbulence transport equations was accomplished by means of the Patankar–Spalding [20] finite-difference procedure. Sharma [42] has employed the same method to obtain predictions of the development of a wall jet over cones of various apex angles. In addition to equations for mean momentum, turbulence energy and dissipation rate, the conservation equation for chemical species was also solved to calculate the dispersion of a tracer of foreign gas in the injectant stream. Fig. 3.2 shows the variation with distance along the cone surface of the maximum velocity in the wall jet, U_m normalized by the velocity at the exit slot, U_e. For both 11° and 90° half-cone angles, the predicted rate of decay of U_m corresponds closely with the measured variation. This behaviour is quite in contrast with the mixing-length predictions: use of the mixing-length distribution required to give correct prediction on a plane surface leads to a serious underestimate of the diminution rate of U_m on the conical surfaces.

3.3. Flow in a pipe

Predictions are shown in figs. 3.3 and 3.4 of two further boundary-layer flows. In these examples, the wall functions presented in (2.3–1) do not provide appropriate boundary conditions. The finite-difference computations have therefore been carried right to the surface, with the use of the low-Reynolds-number form of the model presented in sec. 2.3–2. Again the Patankar–Spalding procedure has been used to solve the equations but the incursion into the viscous and transitional regions requires the use of nearly 100 cross-stream grid points for computational accuracy within 1% (about four times as many as when the wall-function method is used).

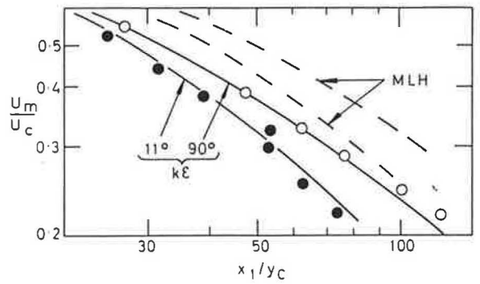

Fig. 3.2. Decay of wall jet on conical surfaces, Sharma (1972).

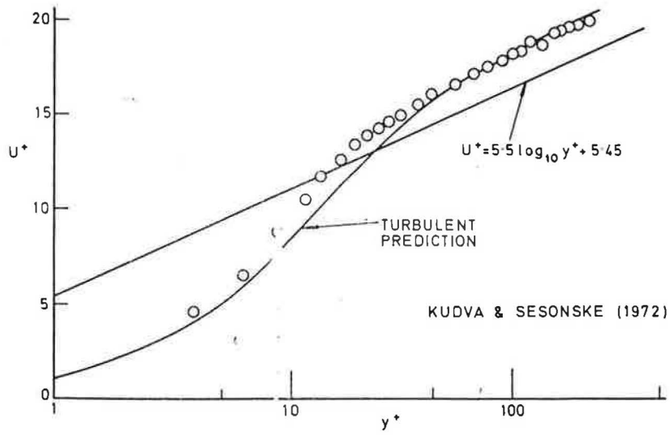

Fig. 3.3a. Pipe-flow velocity profile: $Re = 6000$.

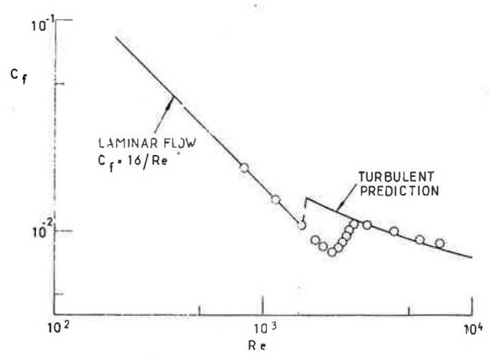

Fig. 3.3b. Friction factor in pipe flow at low Re.

Fully-developed flow in a pipe is considered in fig. 3.3; the low-Reynolds-number end of the turbulent-flow regime is the region here under consideration. Fig. 3.3a shows the mean velocity profile across the pipe plotted semi-logarithmically in so-called 'universal' coordinates. The straight line passing diagonally across the figure represents the 'law of the wall' formula, equation (2.1–12); at high Reynolds numbers ($Re > 2\times10^4$) the measured and predicted profiles coincide with this line in the fully turbulent region near the wall. It is in such conditions that it is appropriate to adopt the wall-function formula provided by (2.3–1). The Reynolds number of the experimental data shown in the figure is only 6000 however; we see that the profile lies well above the high-Reynolds-number line. The predictions of Jones and Launder [29] reproduce satisfactorily this departure from the universal behaviour.

Previous predictions of flow in pipes and channels have employed formulae which imply the near-wall region to be independent of the Reynolds number of the flow. If these models are tuned to give correct predictions for $Re > 20{,}000$ the friction factor at low Reynolds numbers is invariably predicted too high. The reason is, as seen above, that the space-average value of U^+ is larger than it would have been had the prediction been tried to equation (2.3–1); the friction coefficient is simply the square of the reciprocal of this average value. Fig. 3.3b shows the low-Re version of the $k \sim \epsilon$ model to give excellent predictions right down to the Reynolds number at which the turbulent flow becomes intermittent (characterized by a level of C_f which falls as Re is decreased).

3.4. The boundary layer on a turbine blade

The example shown in fig. 3.4 considers the prediction of heat-transfer around the pressure surface of a turbine blade. Detailed measurements of heat-transfer coefficients were obtained by Turner [43] for three different levels of turbulence energy upstream of the blade. In this example the computer solutions were started very near the stagnation point with a *laminar* initial boundary layer. The turbulence present in the free stream is able to exert appreciable effect on the boundary-layer development: at the highest level of free-stream turbulence the boundary layer

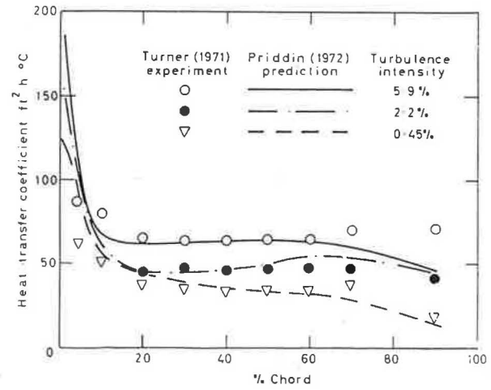

Fig. 3.4. Heat transfer coefficient on pressure surface of gas turbine blade.

has nearly completed the transition to turbulent flow by the end of the blade. At the intermediate turbulence level, the high level of acceleration over the forward portion of the blade inhibits any trend towards an organized turbulent flow until 40% chord; and, for the lowest level of free-stream turbulence, the boundary layer remains laminar throughout. For all three cases the predictions made by Priddin [44] are in extremely close agreement with experiment. It should be emphasized that there has been no explicit specification of when transition will begin in this set of calculations; indeed it may be said that the low-Reynolds-number form of the $k \sim \epsilon$ model has its own built-in 'transition criterion'.

3.5. Film cooling

In the wall-jet flows considered earlier, the lip of the injection slot was thin and the flow was directed smoothly along the wall; consequently the parabolic form of the transport equations could be employed since there were no regions of flow recirculation present. When film-cooling devices are incorporated into combustion chambers, however, they often possess features akin to the wall jets examined theoretically and experimentally by Matthews and Whitelaw [45]: the slot lip is thick and there is an appreciable step in the surface causing a region of reversed flow. An example of the predictions obtained by these workers is provided in fig. 3.5; the ordinate is the adiabatic-wall "effectiveness" and the abscissa is the distance downstream from the injection slot.

These solutions were obtained by means of the elliptic flow finite-difference procedure of Gosman et al. [21]. The use of this numerical solution procedure is common to all the recirculating flow examples presented in this section as is also the employment of the wall-function method for treating the flow adjacent to the wall. In this particular example, however, a modification was found necessary to the practice proposed in sec. 2.3–1. On the downstream face of the step and of the lip (but not elsewhere) the level of ϵ given by equation (2.3–3) was reduced by a factor of 20. The probable cause of the exceptionally low level of dissipation rate there is suggested by

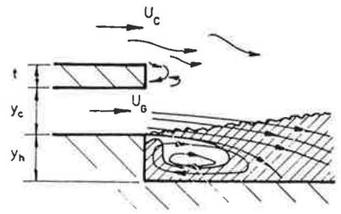

Fig. 3.5a. Wall jet with thick lip and step, character of flow.

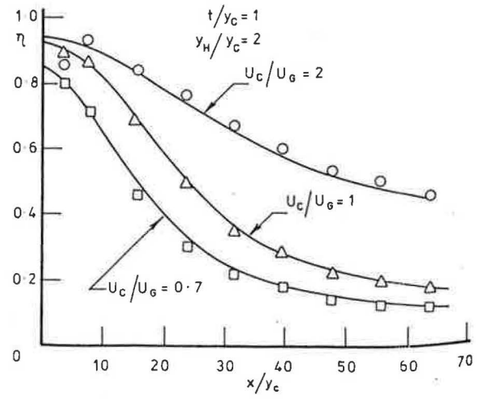

Fig. 3.5b. Decay of wall jet.

fig. 3.5a. By virtue of the recirculating zones, downstream turbulent fluid with large length scale is caused to impinge on the surfaces in question. Because of the very low level of shear stress along these surfaces, the convected fluid is much more influential in determining the local dissipation rate than is the distance from the wall. What is evident from fig. 3.5b is that with this modification, agreement between experiment and prediction is excellent. We should mention that this level of agreement is representative of that obtained for the whole range of flow conditions examined by Matthews and Whitelaw, covering large variations in the ratio of injectant: main stream velocities and densities.

3.6. Coaxial jets

As a further example of an elliptic flow, we consider the devlopment of confined coaxial jets depicted in fig. 3.6a; the velocity ratios are large enough for there to be a recirculating zone present at some position downstream from the jet exit. Fig. 3.6b compares some calculated properties of the recirculating zone with the experimental data of Barchilon and Curtet [46]; the predictions have been obtained by Elghobashi [47]. To conform with the experimental data, the results are presented in terms of the Craya–Curtet parameter defined as:

$$C_t \equiv \frac{U_c}{[(U_i^2 - U_o^2)(r_i/r_o)^2 + \frac{1}{2}(U_o^2 - U_c^2)]^{1/2}} \qquad (3.1\text{–}1)$$

where U_i and U_o are respectively the velocities of the central and annular jets; r_i and r_o are the radii of the jet and the duct; and U_c is defined by:

$$U_c = (U_i - U_o)(r_i/r_o)^2 + U_i \,. \qquad (3.1\text{–}2)$$

It can be seen from fig. 3.6b that the numerical solutions, obtained by means of the procedure of Gosman et al. [21], predict quite well the measured position and magnitude of the recirculating zone over the whole range of C_t covered by the experiments.

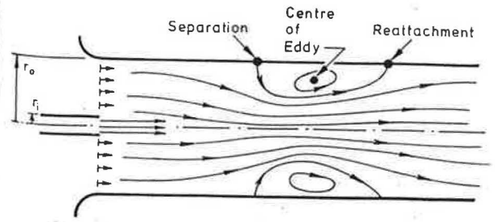

Fig. 3.6a. Character of flow for coaxial ducted jets.

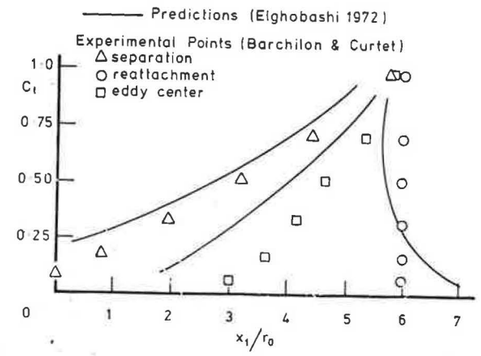

Fig. 3.6b. Properties of recirculation zone in ducted coaxial jets.

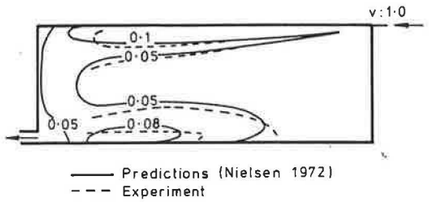

Fig. 3.7. Velocity contours in model auditorium.

3.7. A cavity flow

Fig. 3.7 shows some predictions obtained recently by Nielsen [48] of flow in a rectangular sectioned room; fluid enters the room through a narrow slit in the top right hand corner and leaves at bottom left. Nielsen's particular interest here concerned the problem of ventilating auditoria. To be effective, the ventilating equipment must provide a steady replenishment of air but most not induce velocities so high that the audience feels a draft. There is thus a fairly narrow tolerance on the permissible air velocities near the auditorium floor. It is seen that the velocity contours in this model room are indeed in close agreement with experiment. The result suggests that it would now be fruitful to use the method for extensive design explorations with flows of this type. The cost of such a study would be but a small fraction of that of constructing and instrumenting a model auditorium.

3.8. Flow along a twisted tape

Another flow of great industrial importance is that through tubes with twisted-tape inserts. The purpose of the tape is to impart a swirling motion to the fluid, thereby increasing the surface heat-transfer coefficient. Date [49] has obtained numerical predictions of this flow again by embodying the $k \sim \epsilon$ model into an adaptation of the procedure of Gosman et al. [21]. An example of his predictions is provided by fig. 3.8 which shows the variation of friction factor with Reynolds number for a twist ratio (i.e. the number of pipe diameters for the tape to complete one revolution) of 3.14. In this case agreement with experiment is not so good as in previous examples. Part of the discrepancy may be due to the use of the standard 'equilibrium' wall logarithmic law rather than that given by equation (2.3–1). Probably, however, the main source of disagreement stems from the turbulent viscosity becoming strongly non-isotropic in the complicated strain field of this flow.

3.9. Flow through square-sectioned ducts

In the above example the most promising route for improving predictions seems to be by the use of the algebraic-stress method discussed briefly in sec. 2.4. Certainly this approach has successfully been brought to bear on the problem of flow in ducts of square cross section, where the axial velocity U_1 varies over the cross section in both coordinate directions x_2 and x_3. This strain field gives rise to a turbulent stress field in the plane of the cross section which in turn

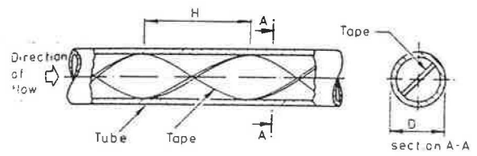

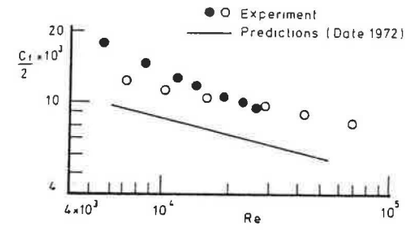

Fig. 3.8. Flow in tubes containing twisted tapes.

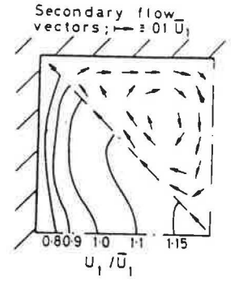

Fig. 3.9. Prediction of fully-developed flow in square-sectioned duct (Tatchell, 1972).

generates a secondary velocity field in this plane. The predictions of Tatchell [50] shown in fig. 3.9 are based on the algebraic stress model and predict very closely the measured secondary flow pattern and its effect on the axial velocity contours. In contrast the $k \sim \epsilon$ model employed with the standard isotropic viscosity relation, equation (2.4–1), leads to the result that there are *no* motions in the plane of the cross section.

4. Concluding remarks

The examples considered in the preceding section convey a representative impression of the capabilities of the $k \sim \epsilon$ model. It is the simplest kind of model that permits prediction of both near-wall and free-shear-flow phenomena without adjustments to constants or functions; it successfully accounts for many low Reynolds-number features of turbulence; and its use has led to accurate predictions of flows with recirculation as well as those of the boundary-layer kind.

Nevertheless the model can still geatly benefit from further improvement and extension. The wall functions used at present are based on the notion that the length scale is a universal function of distance from the wall. Yet the superior predictions given by the low-Reynolds-number version of the model rest squarely on the model's ability to account for the way that accelerations or surface mass transfer *alter* the near-wall length scale. Sometimes, as in the wall jets examined by Matthews and Whitelaw [45], turbulence generated remote from a wall can cause abnormally high levels of length scale near a surface. Urgently needed therefore is a set of wall functions containing the full implications of the low-Reynolds-number form of the model. Indeed there remain many important research tasks concerned with documenting this near-wall region: effects of steep property variation, high Mach numbers, foreign-gas injection, buoyancy and combustion have received little attention in the context of the $k \sim \epsilon$ model.

An equally important research task is that of replacing the isotropic viscosity formula by more

general expressions connecting the stress and strain fields in turbulent flow. As remarked above, there have already been a few successful applications of this approach to flows with more than one significant shear-stress component; in most cases, however, these algebraic-stress formulae give rise to very complicated non-linear equations for the stress components and, for recirculating flows, may seriously complicate the task of solution. There are thus two areas of research implied here. Firstly in the field of numerical analysis, new iteration schemes are needed to promote rapid convergence for even highly non-linear sets of equations. Second, there needs to be a searching set of tests applied to the approximated forms of R_{ij} and ϵ_{ij} appearing in equation (2.4–2); for no one wants to spend extra money and effort using a more elaborate procedure unless he can be sure his predictions will possess greater physical realism than those generated by simpler models.

Acknowledgements

Our thanks are due to our colleagues, Messrs. S. Elghobashi, C.H. Priddin and D.G. Tatchell, for making available to us their as-yet-unpublished predictions based on the $k \sim \epsilon$ model of turbulence.

References

[1] B.E. Launder and D.B. Spalding, Mathematical models of turbulence (Academic Press, London, 1972).
[2] B.E. Launder and D.B. Spalding, Turbulence models and their application to the prediction of internal flows, Heat and Fluid Flow 2 (1972).
[3] F.H. Harlow (Editor), Turbulence transport modelling (AIAA, New York, 1973).
[4] G. Mellor and H.J. Herring, A survey of the mean turbulent field closure models, AIAA Journal 11 (1973) p. 590.
[5] L. Prandtl, Bericht über Untersuchungen zur ausgebildeten Turbulenz, ZAMM 5 (1925) p. 136.
[6] L. Prandtl, Über ein neues Formalsystem für die ausgebildete Turbulenz, Nachrichten von der Akad. der Wissenschaft in Gottingen (1945).
[7] P. Bradshaw, D.H. Ferriss and N.P. Atwell, Calculation of boundary-layer development using the turbulent energy equation, J. Fluid Mechanics 28 (1967) p. 593.
[8] V.W. Nee and L.S.G. Kovasznay, The calculation of the incompressible turbulent boundary layer by a simple theory, Proc. of AFOSR/IFP Conference on Computation of Turbulent Boundary Layers Vol. 1, Stanford University (1968), also Physics of Fluids 12 (1969) p. 473.
[9] A.N. Kolmogorov, Equations of turbulent motion of an incompressible turbulent fluid, Izv. Akad. Nauk SSSR Ser. Phys. VI, No. 1–2 (1942) p. 56.
[10] F.H. Harlow and P. Nakayama, Transport of turbulence energy decay rate, Los Alamos Science Lab., University California Report LA-3854 (1968).
[11] D.B. Spalding, The prediction of two-dimensional, steady turbulent flows, Imperial College, Heat Transfer Section Report EF/TN/A/16 (1969).
[12] W.P. Jones and B.E. Launder, The prediction of laminarization with a 2-equation model of turbulence, International J. Heat & Mass Transfer 15 (1972) p. 301.
[13] P.Y. Chou, On the velocity correlations and the solution of the equations of turbulent fluctuation, Quart. Applied Mathematics 3 (1945) p. 38.
[14] J. Rotta, Statische Theorie nichthomogener Turbulenz, Zeitsch. für Physik 129 (1951) p. 547 and 131 (1951) p. 51.
[15] B.I. Davidov, On the statistical dynamics of an incompressible turbulent fluid, Dokl. ANSSSR 136 (1961) pp. 47–50.
[16] B.A. Kolavandin and I.A. Vatutin, On the statistical theory of non-uniform turbulence, International J. Heat & Mass Transfer 15 (1972) p. 2371.
[17] K. Hanjalić, Two-dimensional asymmetric turbulent flow in ducts, Ph.D. Thesis, University of London (1970).
[18] K. Hanjalić and B.E. Launder, A Reynolds-stress model of turbulence and its application to asymmetric shear flows, J. Fluid Mechanics 52 (1972) p. 609 (Also available as Imperial College, Heat Transfer Section Report TM/TN/A/8).